A multiple mapping conditioning model for differential diffusion

L. Dialameh, M. J. Cleary, and A. Y. Klimenko

Citation: Physics of Fluids (1994-present) **26**, 025107 (2014); doi: 10.1063/1.4864101
View online: http://dx.doi.org/10.1063/1.4864101
View Table of Contents: http://scitation.aip.org/content/aip/journal/pof2/26/2?ver=pdfcov
Published by the AIP Publishing

PHYSICS OF FLUIDS **26**, 025107 (2014)

A multiple mapping conditioning model for differential diffusion

L. Dialameh,[1] M. J. Cleary,[2] and A. Y. Klimenko[1,a)]
[1]*School of Mechanical and Mining Engineering, The University of Queensland, Queensland 4072, Australia*
[2]*School of Aerospace, Mechanical and Mechatronic Engineering, The University of Sydney, New South Wales 2006, Australia*

(Received 15 August 2013; accepted 22 January 2014; published online 12 February 2014)

This work introduces modeling of differential diffusion within the multiple mapping conditioning (MMC) turbulent mixing and combustion framework. The effect of differential diffusion on scalar variance decay is analyzed and, following a number of publications, is found to scale as $Re^{-1/2}$. The ability to model the differential decay rates is the most important aim of practical differential diffusion models, and here this is achieved in MMC by introducing what is called the *side-stepping method*. The approach is practical and, as it does not involve an increase in the number of MMC reference variables, economical. In addition we also investigate the modeling of a more refined and difficult to reproduce differential diffusion effect – the loss of correlation between the different scalars. For this we develop an alternative MMC model with two reference variables but which also makes use of the side-stepping method. The new models are successfully validated against DNS results available in literature for homogenous, isotropic two scalar mixing. © *2014 AIP Publishing LLC*. [http://dx.doi.org/10.1063/1.4864101]

I. INTRODUCTION

Fundamental studies of turbulent mixing are of importance to a broad range of engineering disciplines such as combustion, environmental fluid dynamics, and chemical processing. Due to the complexity of turbulent flows, the majority of fundamental scalar mixing studies consider the evolution of a single scalar only. In practice, of course, more than one scalar is usually mixed. For example, the structure of a turbulent flame is strongly influenced by the complex reactive-diffusive interactions involving numerous chemical species. In general, each scalar has its own molecular diffusivity and may evolve differently to other species due *differential diffusion*. This effect is most noticeable in flows where turbulent mixing is less dominant than molecular mixing, for example, in low Reynolds number flows and small scale mixing processes. Differential diffusion is especially important in mixtures containing species that are substantially more or less diffusive than the other constituents. An example of this latter case is the combustion of hydrogen. Due to the high diffusivity of hydrogen relative to other species (because its much lower molecular weight) and the importance of hydrogen containing species on carbon monoxide oxidation, it is speculated that differential diffusion plays an important role in the burn-out of carbon monoxide (a dangerous pollutant), and also in flame extinction and re-ignition processes which affect combustor stability.[1] The ability to predict these effects is increasingly important as the focus turns to hydrogen containing fuels such as syngas. However, many existing predictive models neglect differential diffusion. This has usually been based on the assumption that turbulent mixing is dominant over molecular mixing thus simplifying the theory behind many turbulent mixing models and becoming an integral part of them. In light of the above discussion it is apparent that this assumption is not valid for all flows thus

a)Electronic mail: a.klimenko@uq.edu.au

motivating several studies to better understand the physics of differential diffusion and to suggest improved predictive models. A brief review follows.

A number of differential diffusion models for transported probability density function (PDF)[2,3] methods are available in the literature. Chen and Chang[1] develop a method for stochastic mixing models and demonstrate its application in the context of the modified Curl's[4] and interaction by exchange with the mean (IEM)[5] mixing models. A differential diffusion form of the Lagrangian spectral relaxation (LSR) model is developed by Fox.[6] More recently McDermott and Pope[7] consider the inclusion of differential spatial diffusion, while Richardson and Chen[8] propose a new approach for treating differential diffusion using both the IEM and Euclidean minimum spanning tree (EMST)[9] micro-mixing models. Various publications consider differential diffusion in the context of other combustion models; Kronenburg and Bilger[10,11] and Smith[12] extend conditional moment closure (CMC)[13] to account for differential diffusion while differential diffusion in flamelet[14,15] models are reported in Pitsch and Peters[16] and Pitsch.[17] Differential diffusion for the linear-eddy model and the eddy-damped quasinormal Markovian (EDQNM) model are developed by Kerstein[18] and Ulitsky *et al.*[19], respectively. Theoretical and DNS investigations of differential diffusion are also widely reported. Following on from Bilger's[20] observation of differential diffusion effects in methane diffusion flames, Bilger and Dibble[21] introduce a differential diffusion variable that is the difference between two mixture fractions (or passive scalars). That quantity is subsequently used by Kerstein *et al.*[22] in their analysis of the Reynolds number scaling of differential diffusion, and in a series of DNS studies by Yeung and co-workers,[23–26] Jaberi *et al.*[27] and Nilsen and Kosály.[28,29] Experimental studies of differential diffusion are reported for both reacting and non-reacting flows. For example, differential diffusion in non-reacting flows is explored by Drake *et al.*[30,31], Masri *et al.*[32], Smith *et al.*[33] and Dibble and Long[34]. While reacting flows are considered by Smith *et al.*[35] and Bergmann *et al.*[36] Most of the above cited works are for non-premixed combustion, which is also the focus of the present research, but it is noted that the effect of differential diffusion on premixed flames are significant and discussed in many publications (e.g., Kuznetsov and Sabelnikov[15]) but not specifically considered here.

In the present work we develop an extension to the multiple mapping conditioning (MMC) model so that it too can account for differential diffusion effects. MMC, which was first derived by Klimenko and Pope,[37] is a modeling framework for turbulent combustion which effectively unifies the features of CMC and PDF models. Deterministic and stochastic formulations of MMC have been derived and tested for various flame configurations; see Cleary and Klimenko[38] for a recent review. The stochastic formulation of MMC is a full-scale PDF method but one where turbulent mixing is local to a low-dimensional reference variable manifold. Mixing localness is a key principle of high quality turbulent mixing models[9] along with other important attributes also satisfied by MMC such as independence, linearity and relaxation to a Gaussian scalar distribution in homogeneous turbulence. For non-premixed combustion of equally diffusing species, it is possible to select a one-dimensional reference variable space representing mixture fraction. This effectively imposes a CMC-type closure onto a PDF model, giving MMC the advantages of both of those methods. MMC models with multiple-dimensional reference variable spaces containing specific enthalpy and scalar dissipation[39] have also been developed for partially premixed combustion.

In general there are two aspects of molecular diffusion in PDF methods which need to be considered: the first is spatial transport,[1,7] which appears in the PDF transport equation as gradient diffusion in physical space; and the second is the process of mixing of scalars at a fixed location,[6,8] which appears as transport in composition space. Differential diffusion may affect both of these. Spatial transport by molecular diffusion can be significant in low Reynolds number turbulent mixing. Moreover, in large eddy simulations (LES) the locally dominant physical processes depend on the filter width and the local viscous length scale. When the filter width becomes small relative to the viscous scale, molecular diffusion needs to be considered. While an MMC-consistent treatment of differential spatial transport can be achieved with the use of the shadow position mixing model (SPMM), which has been recently suggested by Pope,[40] the focus of this present study is on the effects of differential diffusion on the local mixing in composition space. We examine one-point joint characteristics and avoid complications associated with inhomogeneity and chemical reactions by considering differential diffusion of unreactive passive scalars in statistically stationary, isotropic

turbulent flow. Two different MMC models for treating differential diffusion are introduced: the first model has one reference variable and is able to predict the differential rate of decay of scalar variances, while the second model which has two reference variables is also able to predict the loss of correlation between differentially diffusing scalar fields.

The remainder of this paper is organized as follows. Fundamentals of differential diffusion are presented in Sec. II, covering the governing scalar transport equations and some new theory on the Reynolds and Schmidt number scaling of differential diffusion. In Sec. III extensions of the MMC model for differential diffusion are developed and validated against DNS results of Yeung and Pope[23] and Yeung and Luo.[26] The dependence of the model parameters on the Reynolds and Schmidt number are also demonstrated. Conclusions are drawn in Sec. IV.

II. FUNDAMENTALS OF DIFFERENTIAL DIFFUSION

In this section we present some fundamentals of turbulent mixing of differentially diffusing scalars. Part A presents the transport equations governing the advection-diffusion of two passive scalars in homogenous turbulent flow, along with equations for the transport of their variances and covariance. In Part B the spectral view of diffusion, in general, and differential diffusion, in particular, is reviewed and in that context we analyze the Reynolds and Schmidt number scaling of differential diffusion.

A. Governing equations

We consider two passive scalars Y_I and Y_{II} in a homogeneous, isotropic turbulent flow with decaying turbulence and without a mean scalar gradient. This latter simplification allows the mean value of each scalar to be taken as zero without a loss of generality. Each scalar has a different molecular diffusivity denoted by D_I and D_{II}, respectively, with corresponding Schmidt numbers Sc_I and Sc_{II}. The fluctuations of each scalar evolve by the advection-diffusion equations,

$$\frac{\partial Y_I}{\partial t} + u_i \frac{\partial Y_I}{\partial x_i} = D_I \frac{\partial^2 Y_I}{\partial x_i \partial x_i}, \tag{1}$$

$$\frac{\partial Y_{II}}{\partial t} + u_i \frac{\partial Y_{II}}{\partial x_i} = D_{II} \frac{\partial^2 Y_{II}}{\partial x_i \partial x_i}, \tag{2}$$

where $u_i = u_i(x)$ is the turbulent velocity field. The mean scalar variances $\langle Y_{\mathrm{I}}^2 \rangle$ and $\langle Y_{\mathrm{II}}^2 \rangle$ decay with time according to

$$\frac{\partial \langle Y_{\mathrm{I}}^2 \rangle}{\partial t} = -2 D_{\mathrm{I}} \left\langle \left(\frac{\partial Y_{\mathrm{I}}}{\partial x_i} \right)^2 \right\rangle = -\chi_{\mathrm{I}}, \tag{3}$$

$$\frac{\partial \langle Y_{\mathrm{II}}^2 \rangle}{\partial t} = -2 D_{\mathrm{II}} \left\langle \left(\frac{\partial Y_{\mathrm{II}}}{\partial x_i} \right)^2 \right\rangle = -\chi_{\mathrm{II}}, \tag{4}$$

where χ_I and χ_{II} are the scalar dissipation rates. The most important joint statistic is the covariance, $\langle Y_{\mathrm{I}} Y_{\mathrm{II}} \rangle$, which evolves according to

$$\frac{\partial \langle Y_{\mathrm{I}} Y_{\mathrm{II}} \rangle}{\partial t} = -2 (D_{\mathrm{I}} + D_{\mathrm{II}}) \left\langle \frac{\partial Y_{\mathrm{I}}}{\partial x_i} \frac{\partial Y_{\mathrm{II}}}{\partial x_i} \right\rangle = -\chi_{\mathrm{I,II}}, \tag{5}$$

where $\chi_{\mathrm{I,II}}$ denotes the joint scalar dissipation. We also make use of the cross-correlation coefficient, $\rho_{\mathrm{I,II}}$, which is defined as

$$\rho_{\mathrm{I,II}} = \frac{\langle Y_{\mathrm{I}} Y_{\mathrm{II}} \rangle}{\left[\langle Y_{\mathrm{I}}^2 \rangle \langle Y_{\mathrm{II}}^2 \rangle \right]^{1/2}}. \tag{6}$$

B. Reynolds and Schmidt number scaling of differential diffusion

In this section we first review the general spectral properties of turbulent scalar mixing before looking specifically at the spectra of two differentially diffusing scalars. Whereas much previous literature[21,28,6,19,22] has chosen to quantify differential diffusion in terms of the difference of two passive scalars, we instead quantify differential diffusion in terms of the ratio of scalar dissipation timescales. The advantage is that this quantity is stationary in time. We develop relations for the Reynolds and Schmidt number scaling of the differential timescale ratio and make comparison to the scaling that is suggested in the previous literature.

The characteristic feature of any turbulent flow is the occurrence of eddies of different length scales. In decreasing order of size the four scales bounding different turbulent energy regimes are: the macroscale (L); the integral scale (l); the Taylor microscale (λ); and the Kolmogorov microscale (η). According to Kolmogorov's eddy cascade theory[41] the kinetic energy contained in the integral scale eddies is transferred down to the Kolmogorov scales where it is dissipated by viscosity. Turbulent fluctuations of transported scalars follow a similar cascade; the scalar variance generated at the large scales is transferred and dissipated by molecular diffusion at either the Batchelor or Oboukov-Corrsin scales depending on whether the molecular diffusivity is relatively larger or smaller than the kinematic viscosity (i.e., Schmidt number dependence). These dissipative length scales (η, η_B, and η_{OC}) and their corresponding wavenumbers (k_K, k_B, and k_{OC}) are as follows:

$$\text{The Kolmogorov scale:} \qquad k_K = \left(\frac{\varepsilon}{\nu^3}\right)^{1/4} = \frac{1}{\eta}, \tag{7}$$

$$\text{The Batchelor scale:} \qquad k_B = \left(\frac{\varepsilon}{\nu D^2}\right)^{1/4} = k_K Sc^{1/2} = \frac{1}{\eta_B}, \tag{8}$$

$$\text{The Oboukov-Corrsin scale} \qquad k_{OC} = \left(\frac{\varepsilon}{D^3}\right)^{1/4} = k_K Sc^{3/4} = \frac{1}{\eta_{OC}}, \tag{9}$$

where ε is the kinetic-energy dissipation rate, ν is the kinematic viscosity, D is the molecular diffusivity, and $Sc = \frac{\nu}{D}$ is the Schmidt number.

Based on Kolmogorov's eddy cascade hypothesis,[41] in the inertial subrange ($k_0 < k < k_K$) the turbulence is unaffected by viscosity and the kinetic energy spectrum scales according to the well-known $k^{-5/3}$ law. The scaling of the turbulent scalar spectrum is Schmidt number dependent. For $Sc < 1$, the scales are ordered as $k_{OC} < k_B < k_K$ and the scalars dissipate at Oboukov-Corrsin scale while the kinetic energy dissipates at the smaller Kolmogorov scale. Following Oboukov[42] and Corrsin[43] the passive scalar variance spectrum in the *inertial-convective* subrange ($k_0 < k < k_{OC}$) also follows a $k^{-5/3}$ rule

$$E_\theta(k) = C_1 \chi \varepsilon^{-1/3} k^{-5/3}, \tag{10}$$

where C_1 is the Oboukov-Corrsin constant. Alternatively, for $Sc > 1$ the wavenumber cut-offs are ordered as $k_K < k_B < k_{OC}$ and the scalar variance dissipates at the Batchelor scale while the turbulent kinetic energy dissipates at the relatively larger Kolmogorov scale. Batchelor[44] predicted that in the *viscous-convective* subrange ($k_{OC} < k < k_B$) the spectrum scales as

$$E_\theta(k) = C_2 \chi \left(\frac{\nu}{\varepsilon}\right)^{1/2} k^{-1}, \tag{11}$$

where C_2 is the Batchelor constant. It is noted that there are differences between gaseous and liquid flows. The former typically have Schmidt numbers of O(1) hence the dissipative Oboukov-Corrsin scale is of the same order as the Kolmogorov scale, and the later typically have Schmidt numbers of O(10^3) hence the scalar dissipation extends to the dissipative Batchelor scale which is much smaller than the Kolmogorov microscale.

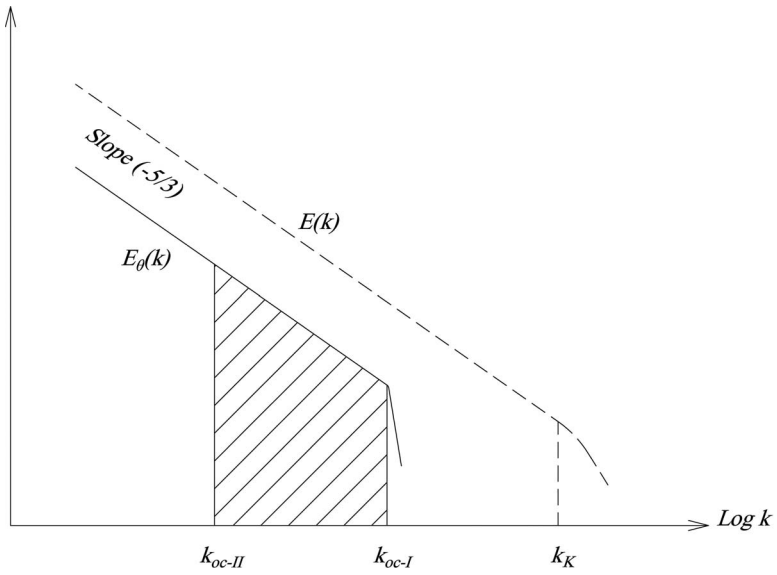

FIG. 1. Energy and variance spectrum of two scalars with different diffusivity for the case $Sc_{II} < Sc_I \leq 1$.

We now consider the spectral properties of two differentially diffusing scalars. For the passive scalars Y_I and Y_{II} introduced in Sec. II A, the scalar dissipation time scales are defined as

$$\tau_I = \frac{2\langle Y_I^2 \rangle}{\chi_I}, \tag{12}$$

$$\tau_{II} = \frac{2\langle Y_{II}^2 \rangle}{\chi_{II}}. \tag{13}$$

In general, two scalars with different dissipation times may have scalar dissipations and scalar variances which are both different. For theoretical analysis, however, it is convenient to consider two scalars with different variances but the same scalar dissipation, $\chi_I = \chi_{II} = \chi$. Figure 1 illustrates the variance spectrum of the two scalars in the inertial-convective subrange for a low Schmidt number flow with $Sc_{II} < Sc_I \leq 1$. As discussed above, the dissipation occurs at the Oboukov-Corrsin scales denoted in wavenumber space by k_{OC-I} and k_{OC-II}. The scalar variance is equal to the integral over the entire wave number space and therefore the difference between the two scalar variances (the cross-hatched area in Figure 1) is given by

$$\langle Y_I^2 \rangle - \langle Y_{II}^2 \rangle = \int_{k_{OC-II}}^{k_{OC-I}} E_\theta(k)\, dk. \tag{14}$$

Now, by substituting $E_\theta(k)$ from Eq. (10) into Eq. (14) we get

$$\langle Y_I^2 \rangle - \langle Y_{II}^2 \rangle = \frac{3}{2} C_1 \chi \varepsilon^{-1/2} \nu^{1/2} \left(Sc_{II}^{-1/2} - Sc_I^{-1/2} \right). \tag{15}$$

Further, by substituting $\varepsilon = u^3/l$, $\nu = ul/\mathrm{Re}_l$ and $T_l = l/u$ into Eq. (15), where u is the turbulent velocity, l is the integral length scale, Re_l is the integral Reynolds number, and T_l is the integral time scale, and dividing the result by χ we get

$$\frac{\langle Y_I^2 \rangle}{\chi} - \frac{\langle Y_{II}^2 \rangle}{\chi} = \frac{3}{2} C_1 T_l \mathrm{Re}_l^{-1/2} \left(Sc_{II}^{-1/2} - Sc_I^{-1/2} \right). \tag{16}$$

Next, substituting Eqs. (12) and (13) on the left side of Eq. (16) then dividing both sides by T_l yields

$$\frac{\tau_I - \tau_{II}}{T_l} = 3C_1 \mathrm{Re}^{-1/2} \left(Sc_{II}^{-1/2} - Sc_I^{-1/2} \right). \tag{17}$$

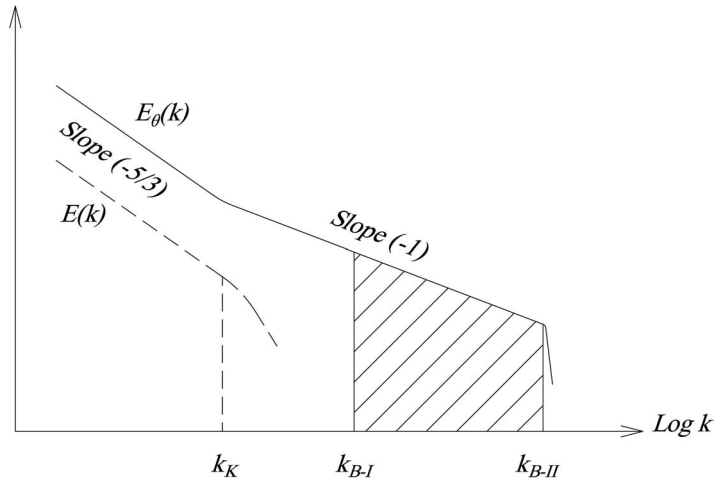

FIG. 2. Energy and variance spectrum of two scalars with different diffusivity for the case $Sc_{II} > Sc_I > 1$.

Without loss of generality, we set $Sc_I = 1$ as a reference value. We also know that at high Reynolds number the ratio of the integral to dissipation timescales, T_l/τ_1, is a constant value[45,46] which we will denote by C_3. With these last two simplifications we finally arrive at a low Schmidt number relationship for the ratio of the dissipation timescales as a function of Reynolds and Schmidt numbers

$$\frac{\tau_{II}}{\tau_I} = 1 - C\mathrm{Re}^{-1/2}\left(Sc_{II}^m - 1\right), \tag{18}$$

where $m = -1/2$ and $C = 3C_1C_3$

We now turn our attention to the high Schmidt number case with $Sc_{II} > Sc_I > 1$. Figure 2 illustrates the variance spectrum $E_\theta(k)$ for this case, showing both the $-5/3$ and -1 spectra and dissipation at the Batchelor scales, k_{B-I} and k_{B-II}. As before, the difference between the two scalar variances (the cross-hatched area in Figure 2) is given by

$$\left\langle Y_{II}^2\right\rangle - \left\langle Y_I^2\right\rangle = \int_{k_{B-I}}^{k_{B-II}} E_\theta(k)\, dk. \tag{19}$$

Substituting $E_\theta(k)$ from Eq. (11) into Eq. (19) gives

$$\left\langle Y_I^2\right\rangle - \left\langle Y_{II}^2\right\rangle = \frac{1}{2}C_2\chi\varepsilon^{-1/2}\nu^{1/2}\left(\ln(Sc_{II}) - \ln(Sc_I)\right), \tag{20}$$

and putting $\varepsilon = u^3/l$, $\nu = ul/\mathrm{Re}_l$, and $T_l = l/u$ into Eq. (20) and dividing by χ leads to

$$\frac{\left\langle Y_I^2\right\rangle}{\chi} - \frac{\left\langle Y_{II}^2\right\rangle}{\chi} = \frac{1}{2}C_2T_l\mathrm{Re}_l^{-1/2}\left(\ln(Sc_{II}) - \ln(Sc_I)\right). \tag{21}$$

Now, substituting Eqs. (12) and (13) on the left side of Eq. (21) then dividing through by T_l while setting $Sc_I = 1$ (as previously explained) leads to the high Schmidt number relationship for the ratio of the dissipation time as a function of Reynolds and Schmidt numbers

$$\frac{\tau_{II}}{\tau_I} = 1 - C_2\mathrm{Re}^{-1/2}\ln(Sc_{II}). \tag{22}$$

It is interesting to compare the scaling developed above with other forms reported in the literature. We consider only the $Sc < 1$ case which is most typical of combustion gases. First we need to formulate our result in terms of the scalar difference, so following Bilger and Dibble[21] we define

$$z = Y_I - Y_{II}, \tag{23}$$

which is rearranged to

$$Y_I = Y_{II} + z. \tag{24}$$

Since the mean values of Y_I and Y_{II} are zero, the mean value of z is also zero and we simply find the variance of Eq. (24) as

$$\left\langle Y_I^2 \right\rangle = \left\langle Y_{II}^2 \right\rangle + \left\langle z^2 \right\rangle + 2 \left\langle Y_{II} z \right\rangle . \tag{25}$$

Differential diffusion occurs in the wavenumber band that is larger than the dissipative Oboukov-Corrsin scale of the most diffusive scalar. So for the case being considered, fluctuations of z occur mainly for $k > k_{OC-II}$ (see Figure 1). Furthermore, if the hypothesis of stochastic independence of large-scale and small-scale fluctuations in turbulent flows is taken into account,[15] we can assume that $\langle Y_{II} z \rangle \approx 0$ since the fluctuations of z overlap with fluctuations of Y_I but not with the fluctuations of Y_{II} (note that $\langle Y_I z \rangle \neq 0$). Upon substitution of this approximation and $\left\langle Y_{II}^2 \right\rangle / \left\langle Y_I^2 \right\rangle = \tau_{II}/\tau_I$ into Eq. (25) we find that

$$\frac{\tau_{II}}{\tau_I} - 1 \approx \frac{\left\langle z^2 \right\rangle}{\left\langle Y_I^2 \right\rangle}. \tag{26}$$

Finally by substituting Eq. (18) into Eq. (26) we get

$$\frac{\left\langle z^2 \right\rangle}{\left\langle Y_I^2 \right\rangle} \approx C\,\mathrm{Re}^{-1/2} \left(Sc_{II}^m - 1 \right). \tag{27}$$

This $\mathrm{Re}^{-1/2}$ scaling is consistent with the theory developed by Kerstein *et al*[22] and later corroborated by the DNS of Nilsen and Kosály.[28] Reynolds number dependence is also analysed by Fox[6] for the study of differential diffusion in forced homogeneous isotropic turbulence and scales as $\left\langle z^2 \right\rangle \sim \mathrm{Re}^{-0.3}$ which is close to the $-1/2$ theoretical value discussed above. The literature contains far fewer studies of the Schmidt number scaling but the result in Eq. (27) with $m = -1/2$ seems to be consistent with the finding of Ulitsky *et al.*[19]

III. AN MMC MIXING MODEL FOR DIFFERENTIAL DIFFUSION

Extensions of MMC to account for the effects of differential diffusion are developed and tested against DNS data[23,26] for binary mixing of two scalars, Y_I and Y_{II}, with differential diffusivities characterized by Schmidt numbers $Sc_{II} < Sc_I \leq 1$. In Part A we present the basic MMC model. In Part B an extended MMC model with a single reference variable is developed for the prediction of differential decay of scalar variance. In Part C an alternative MMC model with two reference variables is developed. In addition to correct prediction of differential decay of variance this second model can also predict the rate of decorrelation of the differentially diffusing scalars. We also demonstrate correct Schmidt and Reynolds number scaling of the two models. Predictions for both differential decay of scalar variance and the rate of decorrleation are validated against DNS with different Schmidt and Reynolds numbers.[23,26]

A. The basic MMC model

In MMC (as in other PDF methods) the turbulent scalar fields, whose mean and covariance evolves according to Eqs. (3)–(5), are modeled using an ensemble of Pope particles which are notional particles which possess scalar quantities subject to a mixing operation.[47] In homogenous turbulence the passive scalars Y_I and Y_{II} are modeled by a discrete mixing operation. We use the MMC-Curl particle interaction mixing model whereby particles are mixed in pairs and evolve as

$$Y_I^{*,\mathrm{new}} = Y_I^* (1-\alpha) + \hat{Y}_\mathrm{I} \alpha, \tag{28a}$$

$$Y_{II}^{*,\mathrm{new}} = Y_\mathrm{II}^* (1-\alpha) + \hat{Y}_\mathrm{II} \alpha. \tag{28b}$$

Here the asterisk denotes values assigned to individual Pope particles, the acute symbol indicates the two-particle average of the scalars prior to mixing and $\alpha \in [0, 1]$ is the mixing extent which is related to the turbulent mixing timescale. The mixing operation should ideally satisfy the set of principles suggested by Subramaniam and Pope.[9] The most important of these, at least within the

current context, are decay of variance consistent with Eqs. (3) and (4) to a Gaussian distribution, linearity and independence of mixing, and localness in composition space. Traditional mixing models satisfy some but not all of these principles. Curl's model[48] satisfies linearity and independence but violates the localness requirement leading to significant over prediction of conditional fluctuations of reactive scalars in jet flames.[49] EMST is local and predicts Gaussian decay but violates linearity and independence. MMC, on the other hand, satisfies all of these principles. Localness is achieved in MMC by forcing mixing to be between pairs of particles which are local in a reference variable space. The reference variables are modeled to emulate the major statistics of the turbulent scalar fields but, at the same time, they are mathematically independent of the stochastic scalar values Y^*. Different versions of MMC use different types of reference variables; for example, both stochastic Markov processes[37,50] and LES-simulated scalar fields[51] have been previously used to generate the MMC reference variables. In this work the reference variables, ξ, are modeled by Ornstein-Uhlenbeck processes[45] of the following form:

$$d\xi = -\frac{\xi(t)}{\theta}dt + \left(\frac{2}{\theta}\right)^{1/2} dW(t), \tag{29}$$

where W(t) is a Wiener process and θ is the reference variable dissipation timescale.

In most conventional joint PDF models, the dissipation of scalar variance is controlled exclusively by the mixing model in Eq. (28) and the parameter α has a major influence. In this respect MMC is substantially different. Mixing is local within a reference space which has the effect of causing scalar fluctuations to decay towards the scalar mean that is conditionally averaged on that reference space. Therefore the parameter α is linked to what we call the *minor dissipation timescale,* denoted here as τ_D. Following Klimenko's analysis[52] of conditional dissipation in various mixing models, a new parameter γ is defined as

$$\gamma = 1 - (1-\alpha)^2. \tag{30}$$

Its ensemble mean is a function of the numerical time step and minor dissipation timescale

$$\langle\gamma\rangle = \frac{4dt}{\tau_D}. \tag{31}$$

The major dissipation of scalar variance occurs due to the diffusion in reference variable space and the parameter θ in Eq. (29) is called the *major dissipation timescale*. The MMC localness parameter, Λ, is defined as the ratio of the minor to major dissipation timescales, $\Lambda = \tau_D/\theta$. Of course, this interpretation of major and minor scalar fluctuations is made on the assumption that the reference space adequately represents the multidimensional space that is accessed by the fluctuating scalar field. The concepts of major and minor dissipation timescales are discussed in detail in previous publications.[52]

B. An MMC model for predicting differential decay of scalar variance (one reference variable method)

The primary objective of any differential diffusion model, especially those for practical applications, is the ability to model the differential rates of decay of scalar variance. For this purpose we propose an MMC model where the mixing of both Y_I^* and Y_{II}^* is localized in the space of a single reference variable ξ_I which is modeled according to Eq. (29). The major dissipation time scale θ_I is related to the physical dissipation timescale, τ_I; the dissipation timescale for the less diffusive species Y_I^*. Conventionally these two values are close to each other and if θ_I is properly selected (below this is achieved by matching the modeled decay of Y_I^* to DNS data[23]) then the correct evolution of Y_I^* ensues. Since $Sc_{II} < Sc_I$ then $\tau_{II}/\tau_I < 1$ according to Eq. (18). The faster rate of dissipation for Y_{II}^* is modeled by extending the mixing window (the average distance between particles in the reference variable space). Such an extension of the mixing window can be achieved in a number of ways and, generally, the order of mixing of the scalars is not important. In the present work, the mixing window for the more diffusive scalar is enlarged by "side stepping" (explained below). This method is selected for the sake of simplicity and convenience as it uses the same algorithm for particle pair

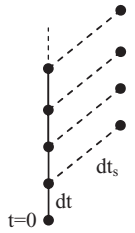

FIG. 3. Conceptual sketch of the side-stepping method.

selection and mixing of both scalars. In this case, however, the order of mixing is fixed as the side step follows the original time step: the more diffusive scalar is mixed after mixing the less diffusive scalar. The full implementation of the model is as follows. The reference variable ξ_I is advanced by a time increment dt at which point scalar Y_I^* is mixed after localizing in ξ_I-space. At that point ξ_I is advanced by a further time increment $dt_s = r_s dt$ at which point scalar Y_{II}^* is localized in the updated ξ_I-space and mixed. That second time increment is a temporary side step and r_s is so called side step parameter in this model. Essentially the side step increases the mixing of the more diffusive scalar by increasing the mixing window or the modeled time available in which mixing takes place. As described below r_s is modeled so that Y_{II}^* evolves correctly. After Y_{II}^* is mixed the side step of ξ_I is discarded and the simulation continues. The process is shown schematically in Figure 3. It is emphasized that only the reference variable is modeled discontinuously and the conservation equations of the physical scalars Y_I and Y_{II} are not violated.

In this model the major dissipation time θ_I determines the variance decay rate of the less diffusive species while r_s determines the differential decay rate and in turn the decay rate of the more diffusive species. For closure, therefore, we require a model for r_s. First, we note the existence of the additional diffusion in reference space, which is associated with mixing. The intensity of this diffusion is given by[53]

$$D_m = \frac{d_m^2}{\tilde{\beta}\tau_D}, \quad \tilde{\beta} = \frac{\langle 1-\alpha^2 \rangle}{\langle 1-\alpha \rangle}, \tag{32}$$

where D_m is the corresponding effective diffusion coefficient and d_m^2 is the square of the characteristic distance between mixing particles. In the side stepping model, there is an increase in the mixing window by an additional side step of dt_s which results in additional stirring of the particles leading to

$$d_m^2 = d_0^2 + 2Bdt_s, \tag{33}$$

where d_0^2 is the average of the square distance between nearest particles. In the present work where a large number of particles are used in order to minimize stochastic errors, we can assume that d_0^2 is negligible in comparison with the term $2Bdt_s$ in Eq. (33). In cases with larger inter-particle spacing, for example, sparse-Lagrangian MMC simulations, the diffusion associated with positive d_0^2 should be taken into account.[47] Hence, additional diffusion is created without varying the mixing extent α. As a result, the effective diffusion coefficient after side stepping and mixing is equal to

$$B_s = B + D_m, \tag{34}$$

where $B = 1/\theta_I$. Substituting Eq. (32) into Eq. (34) where $dt_s = r_s dt$ and τ_D is substituted from Eq. (31) we have

$$\frac{B_s}{B} = \frac{\tau_I}{\tau_{II}} = 1 + r_s \frac{\langle \gamma \rangle}{2\tilde{\beta}}. \tag{35}$$

This last equation is the relationship between scalar dissipation time scale ratio and the side step parameter r_s. From Eq. (18) we see that this ratio is also related to the physical flow properties, characterized by the Reynolds and Schmidt numbers. By substituting Eq. (35) into Eq. (18) the side

stepping parameter is itself related to the flow physics by

$$r_s = \left(\frac{2\tilde{\beta}}{\langle\gamma\rangle}\right)\left(\frac{C\mathrm{Re}^{-1/2}\left(Sc_{II}^{m}-1\right)}{1-\left(C\mathrm{Re}^{-1/2}\left(Sc_{II}^{m}-1\right)\right)}\right). \tag{36}$$

The MMC model developed above is now validated against the DNS data of Yeung and Pope[23] for the binary mixing of two differentially diffusing scalars in statistically stationary, homogeneous, isotropic turbulence. Two different DNS simulations are considered; in the first the scalar pairs have $Sc_I = 1$ and $Sc_{II} = 0.25$ while in the second simulation $Sc_I = 1$ and $Sc_{II} = 0.5$. The flow has a Taylor Reynolds number of $\mathrm{Re}_\lambda = 38$, an integral Reynolds number of $\mathrm{Re}_l = 216.6$ and an eddy turn-over time of 62.5 s. The MMC simulations are performed using 10 000 Pope particles and a numerical time step of 0.1 s. Additional simulations with as many as 30 000 Pope particles and with a numerical time step of 0.01 s indicated that the results are relatively insensitive to changes in the numerical setup. Although a large number of particles are used in these simulations, so that time resolved variances and covariances can be obtained with small stochastic errors, practical implementations of the model within a CFD solver would typically use far few particles. The scalar fields are initialized by $Y_I^* = Y_{II}^*$ and given a standard normal distribution such that $\langle Y_I^*\rangle = \langle Y_{II}^*\rangle = 0$ and $\langle Y_I^{*2}\rangle = \langle Y_{II}^{*2}\rangle = 1$. Similarly, the reference variable is initialized with a standard normal distribution. The MMC localness parameter, Λ, the constant, C, in Eq. (36) and the mixing extent α are the three model parameters requiring explicit selection. The first is a time-invariant quantity whose value can be flow dependent.[52] Here it is selected manually so that the decay of $\langle Y_I^{*2}\rangle$ matches the DNS data while the decay of $\langle Y_{II}^{*2}\rangle$ is modeled implicitly through the side stepping process with r_s given by Eq. (36). The value of α is not critical and any value (or even random values[4]) between 0 and 1 can be used since the other parameters $\langle\gamma\rangle$ and $\tilde{\beta}$ in Eq. (36) will be correspondingly adjusted through Eqs. (30) and (32). The results presented in this work are for $\alpha = 0.02$.

Figure 4 shows the scalar variances versus normalized time which is defined as the simulation time divided the DNS eddy turn-over time. The results for the two simulations with ($Sc_I = 1$, $Sc_{II} = 0.25$) and ($Sc_I = 1$, $Sc_{II} = 0.5$) are shown on the same set of axes. As can be seen the dissipation of scalar fluctuations by mixing occurs at different rates due to their different diffusivities. The results show exponential decay of the variances, indicated by approximately straight lines of constant slope on the linear-log plot. A reasonable match between the MMC predicted decay rate and the DNS data of Yeung and Pope[23] for the first scalar ($Sc_I = 1$) is obtained by setting $\Lambda = 0.1$, which is close the value of 1/8 used by Wandel and Klimenko[50] for a reacting but non-differentially diffusing case. The parameter Λ within the range of 0.5 and 1, is also tested in simulations of Sandia Flame

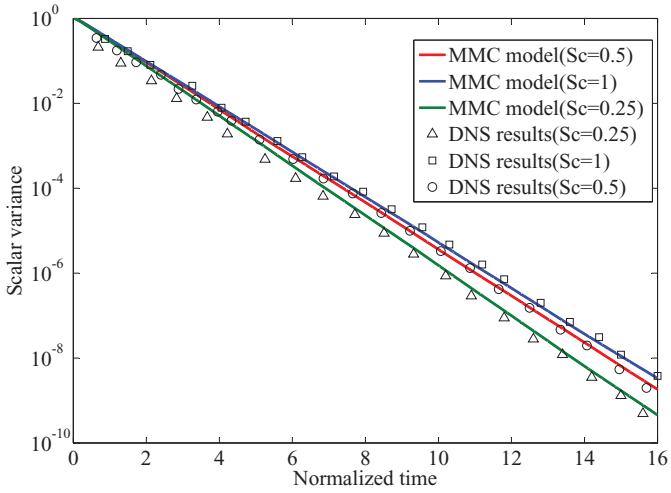

FIG. 4. Scalar variances versus normalized time. Symbols denote DNS data of Yeung and Pope;[23] solid lines denote predictions by the MMC model with one reference variable.

D.[54] To match the decay rate of the second scalar we found that the best match was obtained with $C = 1.24$. Importantly the same set of model parameters are used for the two simulations and the model correctly predicts increasing scalar variance decay with decreasing Schmidt number.

C. An MMC model for predicting differential decay of scalar variance with controlled rate of decorrelation (two reference variable method)

In this section we present a second MMC model which is capable of predicting both the differential scalar variance decay rates (as was the first model) and the rate of decorrelation of those differentially diffusing scalars. The first objective is handled with the side stepping method described in Sec. III B. The second objective, to predict the loss of correlation, is a much more difficult task. We propose a model with two independent reference variables, ζ_I and ζ_{II}, which are related to two independent Ornstein-Uhlenbeck processes, ξ_I and ξ_{II}, modeled according to Eq. (29). We set the major dissipation time scales as $\theta_I = \theta_{II}$. The reference variables are define as functions of ξ_I and ξ_{II}:

$$\zeta_I = \xi_I, \tag{37a}$$

$$\zeta_{II} = f(\xi_I, \xi_{II}). \tag{37b}$$

Mixing occurs by localizing Y_I^* in ζ_I-space and Y_{II}^* in ζ_{II}-space and the function f therefore determines the rate of decorrelation of ζ_I and ζ_{II} and subsequently the decorrelation rate of Y_I^* and Y_{II}^*. A simple linear function is used here

$$\zeta_{II} = f(\xi_I, \xi_{II}) = a\xi_I + b\xi_{II}, \tag{38}$$

where $a = \exp(-\mu t)$ and $b = \sqrt{1 - a^2}$. The parameter μ is called the decorrelation parameter; a value of $\mu = 0$ corresponds to complete correlation of ζ_I and ζ_{II} at all times, while $\mu > 0$ results in an increasing rate of decorrelation. Note that if we set $\mu = 0$ the two-reference variable model is equivalent to the previous one-reference variable model.

The model works as follows. The Ornstein-Uhlenbeck processes ξ_I and ξ_{II} are advanced by a time increment dt at which point scalar Y_I^* is localized in ζ_I-space and mixed. At that point ξ_I and ξ_{II} are advanced by a further time increment $dt_s = r_s dt$ at which point scalar Y_{II}^* is localized in ζ_{II}-space and mixed. As described for the one reference variable model, that second time increment is a temporary side step and after mixing of scalar Y_{II}^* both ξ_I and ξ_{II} are returned to their values prior to the side step. As before, the side step parameter r_s is modeled according to Eq. (36).

The MMC model developed above is once again validated against the DNS data of Yeung and Pope[23] that was described in Sec. III B. In this section we also demonstrate correct scaling with Reynolds number by comparison with the DNS of Yeung and Luo[26] who looked at differentially diffusing scalar pairs ($Sc_I = 1$ and $Sc_{II} = 0.25$) over a range of Taylor Reynolds numbers $\mathrm{Re}_\lambda = 38$, 70, and 90. Unless otherwise noted, the discussion below refers to the DNS of Yeung and Pope[23] with $\mathrm{Re}_\lambda = 38$. As before the MMC simulations are performed using 10 000 Pope particles and a numerical time step of 0.1 s.

Figure 5 shows the scalar variances versus normalized time for two scalars with $Sc_I = 1$ and $Sc_{II} = 0.25$. As for the one reference variable model the best results are found by setting $\Lambda = 0.1$ and $C = 1.24$. Note that this simulation covers a longer time duration than does the previous result shown in Figure 4, but the inset in Figure 5 shows the initial period for which DNS data are available.

We now analyse the scalar decorrelation. Figure 6 shows a scatter plot of Y_{II}^* versus Y_I^* for two scalars with $Sc_I = 1$ and $Sc_{II} = 0.25$ at 80 eddy turn-over times. This result is for a simulation with the decorrelation parameter set to $\mu = 5 \times 10^{-5}$. Initially the two scalars are fully correlated and collapse to the red dashed line which has a slope of unity. Over time the scalars become decorrelated due to the action of differential diffusion as represented by the scatter data and the solid green mean line with a slope less than one. A more quantitative perspective of the decorrelation is found in Figures 7–9. Figure 7 shows DNS data and model results for the correlation coefficient $\rho_{I,II}$ that is

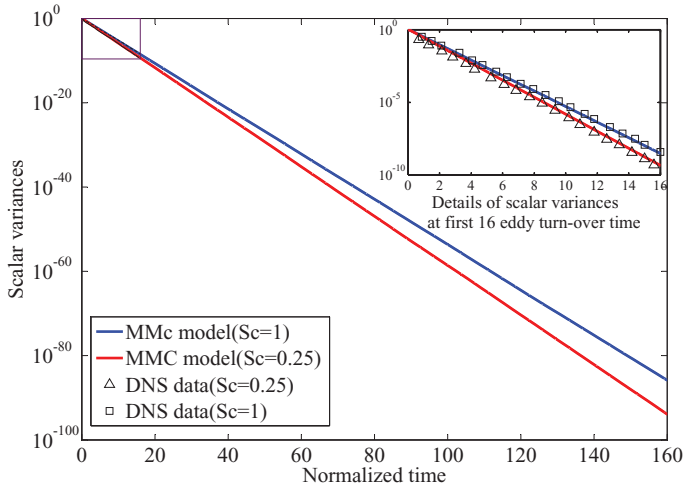

FIG. 5. Scalar variances versus normalized time. Symbols denote DNS data of Yeung and Pope;[23] solid lines denote predictions by the MMC model with two reference variables.

defined in Eq. (6) for two scalar pairs ($Sc_I = 1$, $Sc_{II} = 0.25$) and ($Sc_I = 1$, $Sc_{II} = 0.5$). Modelling is performed for five different values of μ. As expected $\mu = 0$ results in full correlation at all times. As previously mentioned the two reference variable model with $\mu = 0$ is equivalent to the one reference variable model. In this situation, although that model can accurately predict the differential decay of scalar variance, the scalars remain fully correlated which is counter to physical expectations. As μ is increased, the rate of decorrelation also increases. The best results for this particular flow are obtained by setting $\mu = 5 \times 10^{-5}$ for ($Sc_I = 1$, $Sc_{II} = 0.25$) and $\mu = 1.4 \times 10^{-5}$ for ($Sc_I = 1$, $Sc_{II} = 0.5$) while $\mu = 5 \times 10^{-6}$ yields excessively slow rate of decorrelation and $\mu = 5 \times 10^{-4}$ gives a decorrelation time that is an order of magnitude smaller than the DNS decorrelation time. Figure 8 illustrates the evolution of the cross-correlation coefficient $\rho_{I,II}$ for two scalars with ($Sc_I = 1$, $Sc_{II} = 0.25$) at three different Reynolds numbers ($\mathrm{Re}_\lambda = 38$, 70, and 90). Here the model results are compared with the DNS of Yeung and Luo[26] who reported scalar decorrelation rates for

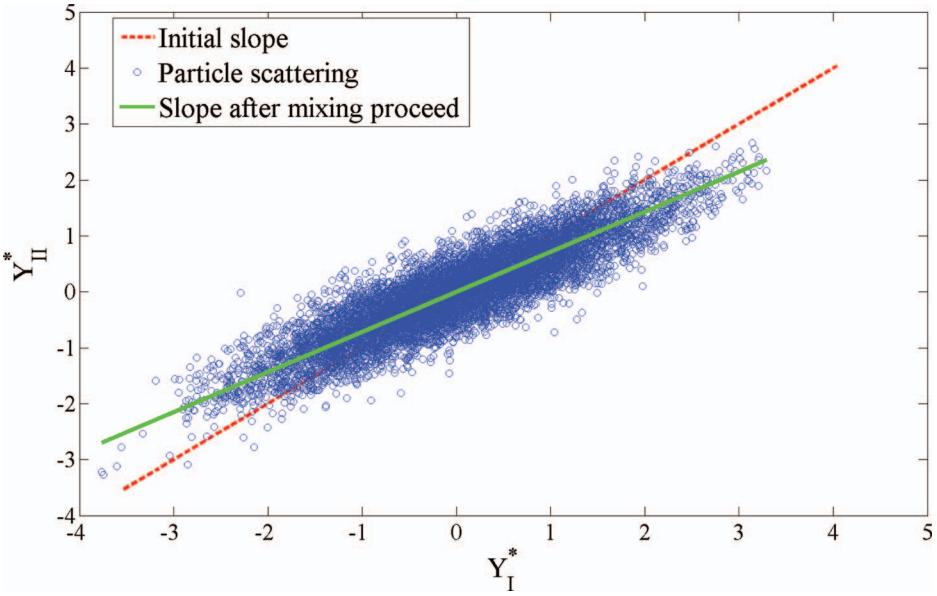

FIG. 6. Particle scatter plot of Y^*_{II} versus Y^*_I at normalized time $t^* = 80$.

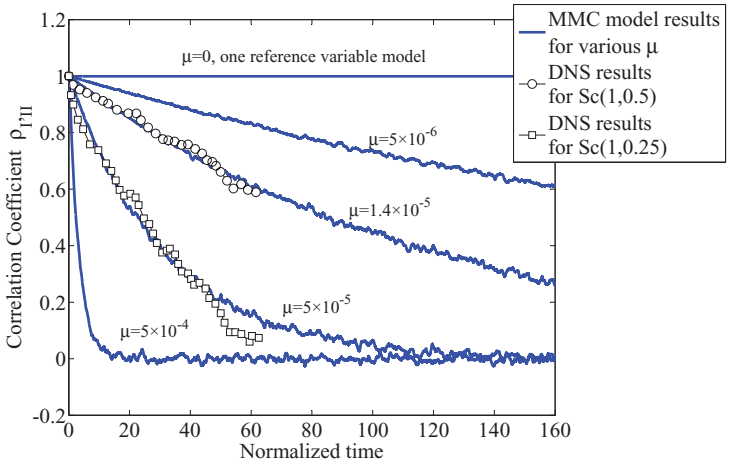

FIG. 7. Evolution of the cross-correlation coefficient $\rho_{I,II}$ for different values of μ. Symbols denotes DNS data of Yeung and Pope;[23] Blue solid lines denote predictions by the MMC model with two reference variables.

three different Reynolds numbers (but not the scalar variance decay rates). An appropriate agreement with DNS results for $\mathrm{Re}_\lambda = 38$, 70, and 90 are achieved by setting $\mu = 2.2 \times 10^{-5}$, 3×10^{-5}, and 5×10^{-5}, respectively. The cross-correlation coefficient of two reference variables ζ_I and ζ_{II} is denoted by $\rho^{\zeta}_{I,II}$ and defined similarly to $\rho_{I,II}$ in Eq. (6). It should be noted that the initial value of$\rho^{\zeta}_{I,II}$ is slightly reduced in high Re simulations to account for the short initial adjustment of the scalar field in DNS.[26] From this simulation data, the decay rate of the scalar correlation coefficients can be scaled as $\mu \sim \mathrm{Re}^{-0.5}$ which is close to the $\rho^{-1}\mathrm{d}\rho/\mathrm{dt} \sim \mathrm{Re}^{-0.3}$scaling suggested by Fox.[6] It is clear from the results that the model correctly predicts a reduced rate of scalar decorrelation with increasing Reynolds number; which of course is indicative of the fact that differential diffusion is weaker at higher Reynolds number.

It is worthwhile to note the mechanism by which decorrelation of Y^*_I and Y^*_{II} is achieved in the model. The principles of MMC allow us to enforce the desirable decorelation rate on the simulated scalars without altering scalar values during mixing or adding any false source terms that can compromise the conservative properties of the model. The scalars simply follow the decorrelation properties directly enforced on the reference variables ζ_I and ζ_{II}. The model directly controls

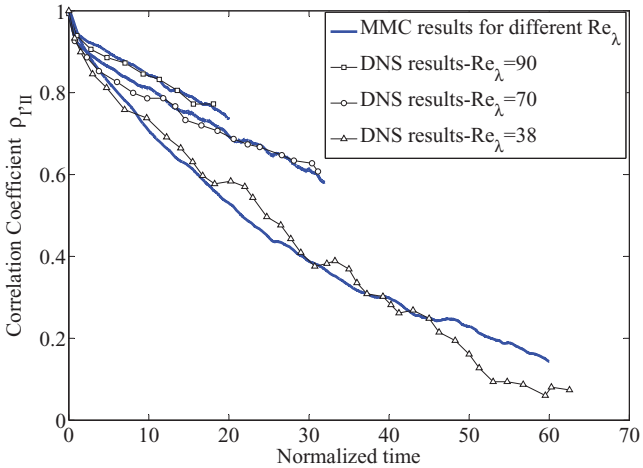

FIG. 8. Evolution of the cross-correlation coefficient $\rho_{I,II}$ between two scalars ($Sc_I = 1$, $Sc_{II} = 0.25$) for three different Reynolds numbers. Symbols denote DNS data of Yeung and Luo[26] while solid lines denote predictions by the MMC model with two reference variables.

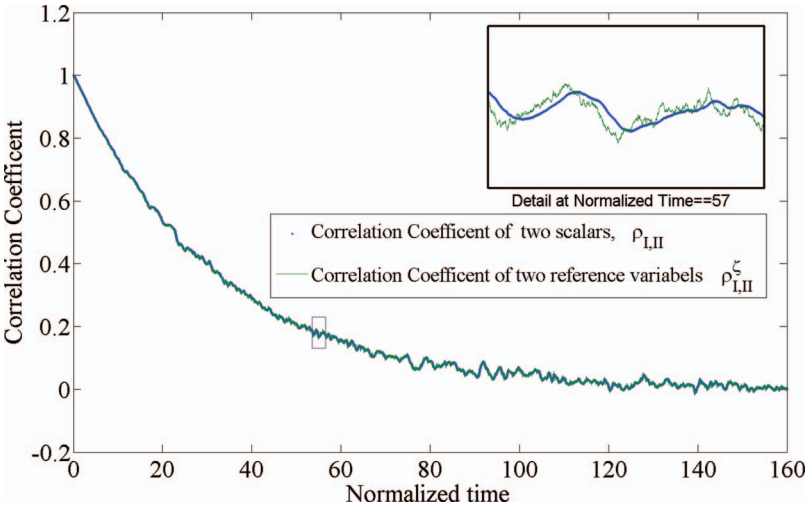

FIG. 9. Evolution of the cross-correlation coefficients $\rho_{I,II}$ and $\rho^{\zeta}_{I,II}$ versus normalized time.

$\rho^{\zeta}_{I,II}$, the cross-correlation coefficient between two reference variables ζ_I and ζ_{II}. Figure 8 shows the evolution of both cross-correlation coefficients against normalized time for the case ($Sc_I = 1$, $Sc_{II} = 0.25$) with $\mu = 5 \times 10^{-5}$. The two values are closely aligned but as the inset figure taken at 57 eddy turn-over times shows $\rho^{\zeta}_{I,II}$ does have some scattering around $\rho_{I,II}$.

IV. CONCLUSION

The current work focuses on spatially homogeneous effects of differential diffusion and on their modelling within the MMC framework. First, the effects of differential diffusion are evaluated theoretically and in comparison with published experimental and DNS data. The dissipation time ratio is found to be proportional to $\mathrm{Re}^{-1/2}$. Second, the standard MMC model is modified to emulate the effects of differential diffusion.

The MMC mixing model is used to account for two important differential diffusion effects by using the reference variable concept. The difference in variance decay rates of two scalars with different diffusivities, which is the primary effect that is desired in practical simulations of differential diffusion, is modeled by using MMC with one reference variable. The concept of side-stepping which leads to an increase in the mixing window is discussed and shown to be a practical and effective approach for modeling differential decay rates without need for a second reference variable. In this one reference variable MMC model the key parameter for controlling the difference in scalar decay rates have been linked to the ratio of the physical dissipation time scales. The second model, MMC with two reference variables, illustrates MMC's capability of modeling the more refined process of scalar decorrelation due to differential diffusion, while at the same time continued to accurately predict the difference in variance decay rates. By enforcing the appropriate correlation rates on two stochastically independent reference variables, the required decorrelation characteristics are automatically enforced by MMC on the simulated scalars. This is done without compromising integrality and universality of the mixing operator. The models are validated against DNS data for joint mixing of two scalars and the level of agreement is very good. In line with the theoretical developments, the models are also found to reflect correctly the Reynolds numbers dependence of the differential diffusion.

Future work will focus on the application of the new models for inhomogeneous shear flows.

ACKNOWLEDGMENTS

This research is supported by the Australian Research Council under Grant No. DP120102294.

[1] J. Y. Chen and W. C. Chang, "Modeling differential diffusion effects in turbulent nonreacting/reacting jets with stochastic mixing models," Combust. Sci. Technol. **133**(4–6), 343–375 (1998).
[2] S. B. Pope, "PDF methods for turbulent reactive flows," Prog. Energy Combust. Sci. **11**(2), 119–192 (1985).
[3] D. C. Haworth, "Progress in probability density function methods for turbulent reacting flows," Prog. Energy Combust. Sci. **36**(2), 168–259 (2010).
[4] J. Janicka, W. Kolbe, and W. Kollmann, "Closure of the Transport Equation for the Probability Density Funcfion of Turbulent Scalar Fields," J. Non-Equilib. Thermodyn. **4**, 47 (1979).
[5] C. Dopazo and E. E. O'Brien, "An approach to the autoignition of a turbulent mixture," Acta Astronaut. **1**(9–10), 1239–1266 (1974).
[6] R. O. Fox, "The Lagrangian spectral relaxation model for differential diffusion in homogeneous turbulence,"Phys. Fluids **11**(6), 1550 (1999).
[7] R. McDermott and S. B. Pope, "A particle formulation for treating differential diffusion in filtered density function methods,"J. Comput. Phys. **226**(1), 947–993 (2007).
[8] E. S. Richardson and J. H. Chen, "Application of PDF mixing models to premixed flames with differential diffusion," Combust. Flame **159**(7), 2398–2414 (2012).
[9] S. Subramaniam and S. B. Pope, "A mixing model for turbulent reactive flows based on Euclidean minimum spanning trees," Combust. Flame **115**(4), 487–514 (1998).
[10] A. Kronenburg and R. W. Bilger, "Modelling of differential diffusion effects in nonpremixed nonreacting turbulent flow," Phys. Fluids **9**(5), 1435 (1997).
[11] A. Kronenburg and R. W. Bilger, "Modelling differential diffusion in nonpremixed reacting turbulent flow: Application to turbulent jet flames," Combust. Sci. Technol. **166**(1), 175–194 (2001).
[12] N. S. A. Smith, *1999 Australian Symposium on Combustion and Sixth Australian Flame Days* (University of Newcastle, Australia, 1999), pp. 61–65.
[13] A. Y. Klimenko and R. W. Bilger, "Conditional moment closure for turbulent combustion," Prog. Energy Combust. Sci. **25**(6), 595–687 (1999).
[14] N. Peters, "Laminar diffusion flamelet models in non-premixed turbulent combustion," Prog. Energy Combust. Sci. **10**(3), 319–339 (1984).
[15] V. R. Kuznetsov and V. A. Sabel'nikov, *Turbulence and Combustion* (Hemisphere Publishing Corporation, 1990).
[16] H. Pitsch and N. Peters, "A consistent flamelet formulation for non-premixed combustion considering differential diffusion effects," Combust. Flame **114**(1–2), 26–40 (1998).
[17] H. Pitsch, "Unsteady flamelet modeling of differential diffusion in turbulent jet diffusion flames," Combust. Flame **123**(3), 358–374 (2000).
[18] A. R. Kerstein, "Linear-eddy modelling of turbulent transport. Part 3. Mixing and differential molecular diffusion in round jets," J. Fluid Mech. **216**, 411–435 (1990).
[19] M. Ulitsky, T. Vaithianathan, and L. R. Collins, "A spectral study of differential diffusion of passive scalars in isotropic turbulence," J. Fluid Mech. **460**, 1–38 (2002).
[20] R. W. Bilger, "Reaction rates in diffusion flames," Combust. Flame **30**, 277–284 (1977).
[21] W. Bilger and R. W. Dibble, "Differential molecular diffusion effects in turbulent mixing," Combust. Sci. Technol. **28**(3–4), 161–172 (1982).
[22] A. R. Kerstein, M. A. Cremer, and P. A. McMurtry, "Scaling properties of differential molecular diffusion effects in turbulence," Phys. Fluids **7**(8), 1999 (1995).
[23] P. K. Yeung and S. B. Pope, "Differential diffusion of passive scalars in isotropic turbulence," Phys. Fluids A **5**(10), 2467–2478 (1993).
[24] P. K. Yeung, "Multi-scalar triadic interactions in differential diffusion with and without mean scalar gradients," J. Fluid Mech. **321**, 235–278 (1996).
[25] P. K. Yeung, M. C. Sykes, and P. Vedula, "Direct numerical simulation of differential diffusion with Schmidt numbers up to 4.0," Phys. Fluids **12**(6), 1601 (2000).
[26] P. K. Yeung and B. Luo, *Proceedings of the 10th Symposium on Turbulent Shear Flows* (University Park, PA, 1995), pp. 31–37.
[27] F. A. Jaberi, R. S. Miller, F. Mashayek, and P. Givi, "Differential diffusion in binary scalar mixing and reaction," Combust. Flame **109**(4), 561–577 (1997).
[28] V. Nilsen and G. Kosály, "Differentially diffusing scalars in turbulence," Phys. Fluids **9**(11), 3386 (1997).
[29] V. Nilsen and G. Kosály, "Differential diffusion in turbulent reacting flows," Combust. Flame **117**(3), 493–513 (1999).
[30] M. C. Drake, R. W. Pitz, and M. Lapp, "Laser measurements on nonpremixed & air flames for assessment of turbulent combustion models," AIAA J. **24**(6), 905–917 (1986).
[31] M. C. Drake, M. Lapp, C. M. Penney, S. Warshaw, and B. W. Gerhold, "Measurements of temperature and concentration fluctuations in turbulent diffusion flames using pulsed raman spectroscopy," Symp. (Int.) Combust. **18**(1), 1521–1531 (1981).
[32] A. R. Masri, R. W. Dibble, and R. S. Barlow, "Chemical kinetic effects in nonpremixed flames of H2/CO2 fuel," Combust. Flame **91**(3–4), 285–309 (1992).
[33] L. L. Smith, R. W. Dibble, L. Talbot, R. S. Barlow, and C. D. Carter, "Laser Raman scattering measurements of differential molecular diffusion in nonreacting turbulent jets of H2/CO2 mixing with air," Phys. Fluids **7**(6), 1455 (1995).
[34] R. Dibble and M. Long, "Investigation of differential diffusion in turbulent jet flows using planar laser Rayleigh scattering," Combust. Flame **143**(4), 644–649 (2005).
[35] L. L. Smith, R. W. Dibble, L. Talbot, R. S. Barlow, and C. D. Carter, "Laser Raman scattering measurements of differential molecular diffusion in turbulent nonpremixed jet flames of H2CO2 fuel," Combust. Flame **100**(1–2), 153–160 (1995).

[36] V. Bergmann, W. Meier, D. Wolff, and W. Stricker, "Application of spontaneous Raman and Rayleigh scattering and 2D LIF for the characterization of a turbulent CH4/H2/N2 jet diffusion flame," Appl. Phys. B **66**(4), 489–502 (1998).
[37] A. Y. Klimenko and S. B. Pope, "The modeling of turbulent reactive flows based on multiple mapping conditioning," Phys. Fluids **15**(7), 1907 (2003).
[38] M. J. Cleary and A. Y. Klimenko, in *Turbulent Combustion Modeling: Advances, New Trends and Perspectives*, edited by T. Echekki and E. Mastorakos (Springer, Netherlands, 2011).
[39] A. Kronenburg and M. J. Cleary, "Multiple mapping conditioning for flames with partial premixing," Combust. Flame **155**(1–2), 215–231 (2008).
[40] S. B. Pope, "A model for turbulent mixing based on shadow-position conditioning," Phys. Fluids **25**, 110803 (2013).
[41] A. N. Kolmogorov, "The local structure of turbulence in incompressible viscous fluid for very large reynolds numbers," Proc.: Math. Phys. Sci. **434**(1890), 9–13 (1991).
[42] A. M. Oboukov, "Structure of the temperature field in a turbulent flow," Izv. Akad. Nauk SSSR, Geogr. Geofiz. **13**, 58–69 (1949).
[43] S. Corrsin, "On the spectrum of isotropic temperature fluctuations in an isotropic turbulence," J. Appl. Phys. **22**, 469 (1951); "Erratum: On the spectrum of isotropic temperature fluctuations in an isotropic turbulence," J. Appl. Phys. **22**(10), 1292 (1951).
[44] G. K. Batchelor, "Small-scale variation of convected quantities like temperature in turbulent fluid Part 1. General discussion and the case of small conductivity," J. Fluid Mech. **5**(01), 113–133 (1959).
[45] S. B. Pope, *Turbulent Flows* (Cambridge University Press, 2000).
[46] P. A. Durbin and B. Pettersson-Reif, *Statistical Theory and Modeling for Turbulent Flows* (Wiley, 2011).
[47] A. Y. Klimenko and M. J. Cleary, "Convergence to a model in sparse-Lagrangian FDF simulations," Flow, Turbul. Combust. **85**(3–4), 567–591 (2010).
[48] R. L. Curl, "Dispersed phase mixing: I. Theory and effects in simple reactors," AIChE J. **9**(2), 175–181 (1963).
[49] M. J. Cleary and A. Y. Klimenko, "A detailed quantitative analysis of sparse-Lagrangian filtered density function simulations in constant and variable density reacting jet flows," Phys. Fluids **23**(11), 115102 (2011).
[50] A. P. Wandel and A. Y. Klimenko, "Testing multiple mapping conditioning mixing for Monte Carlo probability density function simulations," Phys. Fluids **17**(12), 128105 (2005).
[51] Y. Ge, M. J. Cleary, and A. Y. Klimenko, "Sparse-Lagrangian FDF simulations of Sandia Flame E with density coupling," Proc. Combust. Inst. **33**(1), 1401–1409 (2011).
[52] A. Klimenko, "Matching conditional moments in PDF modelling of nonpremixed combustion," Combust. Flame **143**(4), 369–385 (2005).
[53] A. Y. Klimenko, "On simulating scalar transport by mixing between Lagrangian particles," Phys. Fluids **19**(3), 031702 (2007).
[54] K. Vogiatzaki, A. Kronenburg, S. Navarro-Martinez, and W. P. Jones, "Stochastic multiple mapping conditioning for a piloted, turbulent jet diffusion flame," Proc. Combust. Inst. **33**(1), 1523–1531 (2011).